Advanced Mechanical and Mechatronic Systems

Research Article
Volume 2(1), 2026, 16–32
https://doi.org/10.53623/amms.v2i1.764

Numerical Study: Crashworthiness of Hydrogen Powered Vehicle in a Collision

Chipego Jacobs, Kyaw Myo Aung*, Sujan Debnath

Department of Mechanical & Mechatronics Engineering, Curtin University Malaysia

*Correspondence: kyawmyoaung@curtin.edu.my

SUBMITTED: 8 July 2025; REVISED: 14 August 2025; ACCEPTED: 18 August 2025

ABSTRACT: This numerical research focuses on the crashworthiness of a hydrogen powered vehicle in a collision including the safety of the hydrogen storage system. The model of the vehicle and the hydrogen storage system were developed in Ansys Space Claim. In another Ansys tool, Mechanical, the simulations for three crash scenarios were conducted. The simulations involved the modelled vehicle with the hydrogen system impacting a rigid wall in frontal, rear and side scenarios to assess the amount of deformation, stress distribution and the internal/total energy absorbed by the tanks. The results from the simulations showed that there was significant deformation and stress experienced by the hydrogen storage system. maximum stress values from the frontal impact were 4630.2 MPa which is way over values of typical failure points of Type IV tanks. From the side impact, it was noted too that the tanks had higher internal energy absorbed when compared to the other 2 scenarios. The recorded value of this amount of energy was 255.32 J and show there is a high risk of the tank rupturing or leaking. The data was analysed with other literature values confirming the found data from the simulations conducted. These findings demonstrate that even though the current configuration of the hydrogen system has less risk of failure from minor impacts, they are still in a state of vulnerability under severe crashes. Furthermore, the findings highlight the continued need of research on improving the configuration of storage systems, better protection systems and inclusion of many more parameters.

KEYWORDS: Hydrogen vehicle; crashworthiness; finite element analysis (FEA)

1. Introduction

Hydrogen fuel cell vehicles were regarded as a promising solution that offered a clean route to a sustainable transportation sector. The technology in these vehicles had the potential to transform travel by addressing the impacts of existing internal combustion engines [1]. A notable issue with hydrogen-powered vehicles was the use of high-pressure hydrogen storage systems. These systems were responsible for storing hydrogen fuel, but they carried serious risks, especially in the event of a crash. Catastrophic failure was likely because the operating pressure of the tanks was approximately 10,000 psi. Hydrogen was also highly flammable, and when released it could result in fires and explosions, making the safety of these systems in crashes crucial.

Hydrogen burned with a flame speed approximately seven times faster than that of natural gas or gasoline, making it more prone to transition into a deflagration or even a detonation compared with other fuels. However, the risk of detonation depended on several complex factors including the fuel-to-air ratio, temperature, and particularly the shape and size of the space containing the hydrogen. In open-air conditions, hydrogen detonation was extremely unlikely. One safety concern was that hydrogen flames were nearly invisible, posing a danger because individuals nearby might not notice the fire. This issue could be mitigated by adding chemicals to the hydrogen to make the flame visible [2].

Using hydrogen as a fuel in vehicles introduced specific safety risks. These risks needed to be evaluated when the vehicle was off, operating normally, or involved in a crash. The main concerns were fire and explosion, though toxicity was not an issue since hydrogen and its combustion products were non-toxic. Fire or explosion hazards could originate from the hydrogen storage tank, supply lines, or the fuel cell. Among these, the fuel cell presented the lowest risk, even though it separated hydrogen and oxygen with a thin polymer membrane (20–30 μm thick). If this membrane ruptured, hydrogen and oxygen could mix, causing the cell to lose voltage, a condition easily detected by monitoring systems, which then shut off the supply lines. Although the operating temperature of the fuel cell (60–90 °C) was not high enough to ignite hydrogen, ignition could still occur on the catalyst surface where hydrogen and oxygen combined. Any potential damage would remain limited due to the small volume of hydrogen in the cell and supply lines [3].

The hydrogen storage tank contained the largest quantity of hydrogen at any given time and was the most critical component in terms of safety. Possible failure scenarios during both normal use and collisions included catastrophic rupture caused by manufacturing defects, mishandling, stress fractures, sharp object punctures, or external fires where the pressure relief valve failed to activate; large-scale leakage resulting from accidental activation of the pressure relief valve, chemical degradation of the tank wall, sharp object penetration, or proper operation of the valve during a fire; and slow leaks caused by stress cracks in the tank lining, defective pressure relief valves, poor connections between the tank and fuel line, or damage to fittings from impacts [4].

Research on the safety and crashworthiness of hydrogen-powered vehicles, particularly hydrogen fuel cell vehicles, remained limited, especially regarding the behavior of storage systems during impacts. Despite prior studies on fossil-fuel-powered vehicles, the findings could not be directly applied to hydrogen vehicles because of the use of hydrogen as fuel and the complex high-pressure storage systems. Hydrogen-powered vehicles, also referred to as hydrogen fuel-cell vehicles (HFCVs), represented a promising alternative to internal combustion engine vehicles and battery-operated electric vehicles (EVs). Through electrochemical reactions between hydrogen and oxygen, HFCVs generated electricity that powered motors, similar to battery electric vehicles. Examples included Toyota’s Mirai and Hyundai’s Nexo. HFCVs demonstrated high energy conversion efficiency compared with traditional vehicles because they achieved longer driving ranges and faster refueling times, which made them practical for public transportation and heavy-duty haulage.

The operation of HFCVs was based on electrochemical reactions occurring in the fuel cell, where hydrogen and oxygen combined to produce electricity that powered the vehicle [5]. Hydrogen gas stored in a high-pressure tank was supplied to the anode side of the fuel

cell. At the anode, hydrogen was ionized on a platinum catalyst, splitting into two protons and two electrons, as shown in Eq. (1) [6].

$$H_2 \rightarrow 2H^+ + 2e^-$$

The protons passed through the proton exchange membrane (PEM), while the electrons moved through an external circuit to the cathode, producing an electric current. At the cathode, oxygen from the air reacted with the protons and electrons to form water, as shown in Eq. (2) [7].

$$O_2 + 4H^+ + 4e^- \rightarrow 2H_2O$$

The flow of electrons generated electricity that powered the electric motors and other vehicle systems (Gurz et al., 2017) [5]. The overall reaction was represented as Eq. (3).

$$H_2 + O_2 = 2H_20 + Electrical\ Energy$$

Finite Element Analysis (FEA) was a powerful technique used to predict the behavior of objects under different physical conditions such as vibrations, heat, fluid flow, and mechanical failures. The method divided complex structures into small elements, allowing engineers to analyze the behavior of materials and integrated structures efficiently. Using FEA to assess vehicle safety was common practice because it shortened development time during early research stages. It also facilitated successive adjustments and improvements, reducing cost and development time [9]. FEA software provided insights into stress distribution, deformation, and failure points affecting occupant safety. It also enabled simulation of dangerous crash scenarios that were impossible or impractical to replicate physically, including frontal, side, rear, and offset collisions [10].

For hydrogen-powered vehicles, FEA offered the same advantages, ensuring structural safety and system performance in crash simulations. It incorporated material properties specific to hydrogen vehicles, allowing realistic modeling of stresses and strains [10]. One study titled *Static and Dynamic Analysis of Hydrogen Fuel Cell City Bus Body Frame* applied FEA to examine the strength and stiffness of a hydrogen-powered bus frame. Static FEA simulations assessed different loading conditions and identified critical stress points. The optimized frame design met requirements and significantly improved safety under dynamic conditions [9].

2. Materials and Methods

The methodology adopted to accomplish the objective of the project was to investigate the crashworthiness of a hydrogen-powered vehicle. The parameters selected in each section complied with the standards recommended by both the National Highway Transportation Safety Administration and the Global Technical Regulations No. 13 (GTR13). These parameters included the type of crash scenario, the boundary conditions applied to the vehicle, and the initial speeds of the vehicle [10–12]. The flowchart illustrating the methodology used in the study was presented in Figure 1.

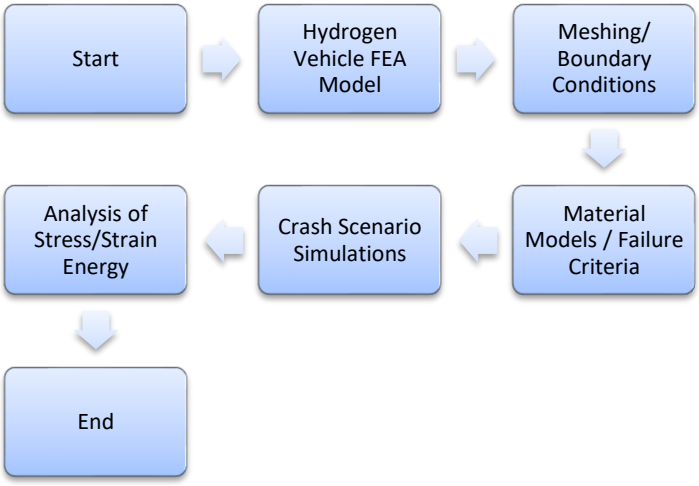

Figure 1. Flowchart of methodology.

2.1.vehicle modelling & meshing.

The preferred software used to carry out the methodology was ANSYS 2024 R2. It provided a comprehensive and dynamic simulation solution with the capability to handle material modeling and impact analysis. The effectiveness of the software allowed for the successful completion of the research. A vehicle model was developed in ANSYS SpaceClaim. The dimensions of the vehicle used to achieve the objectives were outlined in Table 1. These dimensions corresponded to those of a standard sedan vehicle.

Table 1. Vehicle dimensions and material.

Classification	**Values**
Length (mm)	4,890
Wheelbase (mm)	2,780
Width (mm)	3,630
Height (mm)	1,535
Body material	Aluminium Alloy

As for the hydrogen storage tank, it will be cylindrical. Table 2 outlines the hydrogen storage tank parameters that will be considered. These size parameters are standardized and are utilised in the Toyota Mirai second generation [13].

Table 2: High-pressure hydrogen tank specifications.

Classification	Parameter
Tank Type	IV (Plastic liner)
Tank Pressure	70 MPa
Size	Tank 1: Diameter = 299mm, Length = 1,467mm
	Tank 2: Diameter = 299mm, Length = 1,201mm
	Tank 3: Diameter = 299mm, Length = 683.5mm
Internal Volume (L)	64.9
Hydrogen Storage Mass (Kg)	43.0
Regulatory and Standard Compliance	UN-R134

The model setup of the vehicle with the hydrogen storage system was shown in Figure 2. The model was developed as a surface body to represent the actual body of the vehicle. The vehicle model was the same for the frontal, rear, and side impacts. The model was later imported into ANSYS Mechanical for meshing. When imported into ANSYS Workbench and subsequently into ANSYS Mechanical, the model appeared as shown in Figures 3, 4, and 5 for the frontal, rear, and side impacts, respectively.

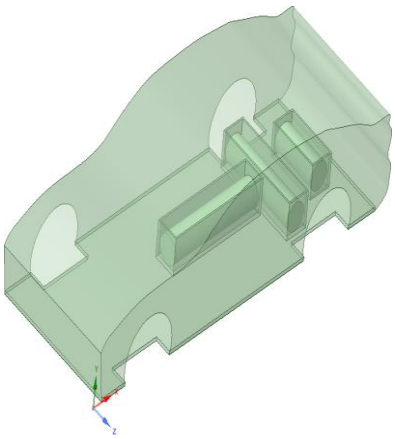

Figure 2. Model of hydrogen vehicle with hydrogen storage system.

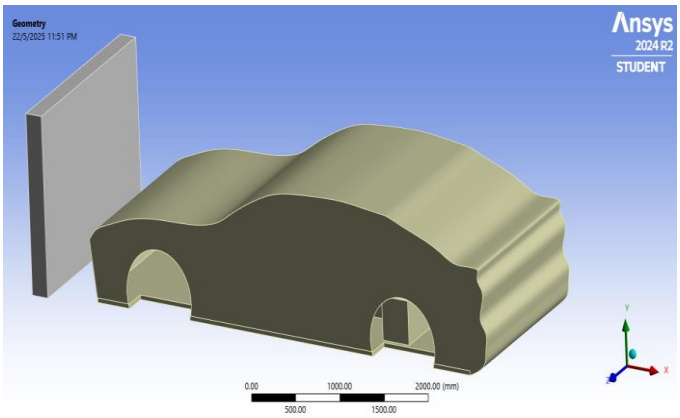

Figure 3. Model of hydrogen powered vehicle with hydrogen storage system (frontal impact).

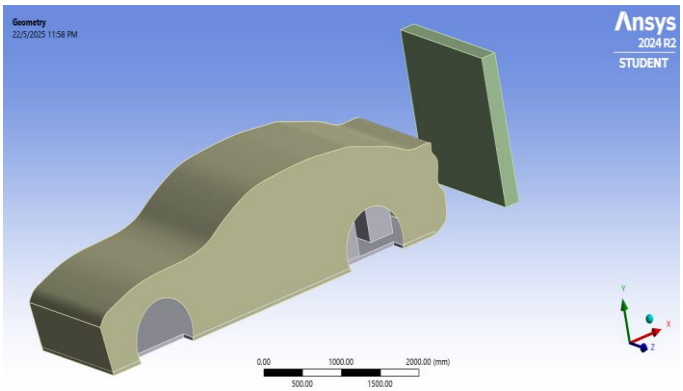

Figure 4. Model of hydrogen powered vehicle with hydrogen storage system (rear impact).

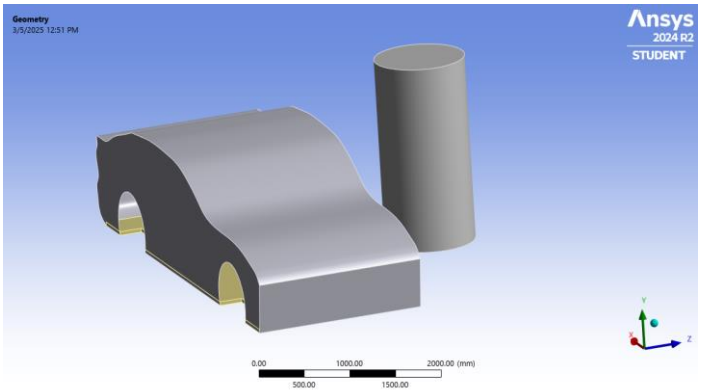

Figure 5. Model of hydrogen powered vehicle with hydrogen storage system (side impact).

The hydrogen storage system, illustrated in Figure 6, was composed of a chassis-like structure and compartments that housed the Type IV storage tanks..

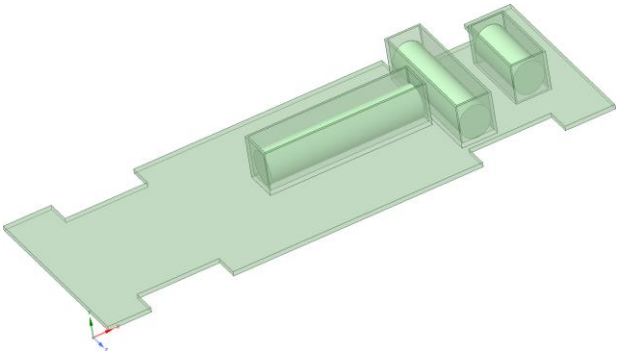

Figure 6. Model of hydrogen storage system.

The system was modeled to closely represent an actual hydrogen-powered vehicle, incorporating parts such as mounts and bulkheads that provided additional protection to the tank system. As shown in Figure 5, three cylinders represented the hydrogen tanks. The next step was the design of a base structure with compartments that allowed placement of the hydrogen tanks, since the parts were not joined in any way. This base also acted as the chassis of the vehicle and absorbed most of the impact before it reached the tanks. This approach allowed a real-life crash scenario to be considered, as vehicles were designed with crumple zones to absorb the majority of the impact during a crash. From the developed model of the vehicle and its components, meshing was conducted within ANSYS Mechanical. The applied mesh used adaptive sizing with a resolution of 6. From the meshed model, the software generated the number of elements and nodes. Figure 7 presented the meshed model of the vehicle with the hydrogen system and the impact wall in the frontal crash scenario. The meshed model comprised of 160198 nodes and 151050 elements. Specifications of the mesh are included in the Table 3.

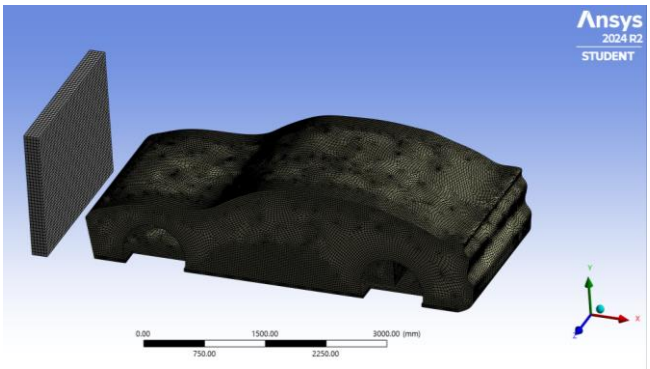

Figure 7. Meshed FE vehicle model and wall.

Table 3. Meshing specifications.

Number of nodes	160198
Number of elements	151050
Minimum Edge Length (mm)	40
Span Angle Centre	Fine
Resolution	6

The same mesh conditions were applied for the rear and side impact scenarios. The rear impact simulation, including the vehicle model and wall, contained 175,825 nodes and 166,564 elements, as shown in Figure 8. For the side impact, the vehicle model and wall contained 218,366 nodes and 208,383 elements, as shown in Figure 9.

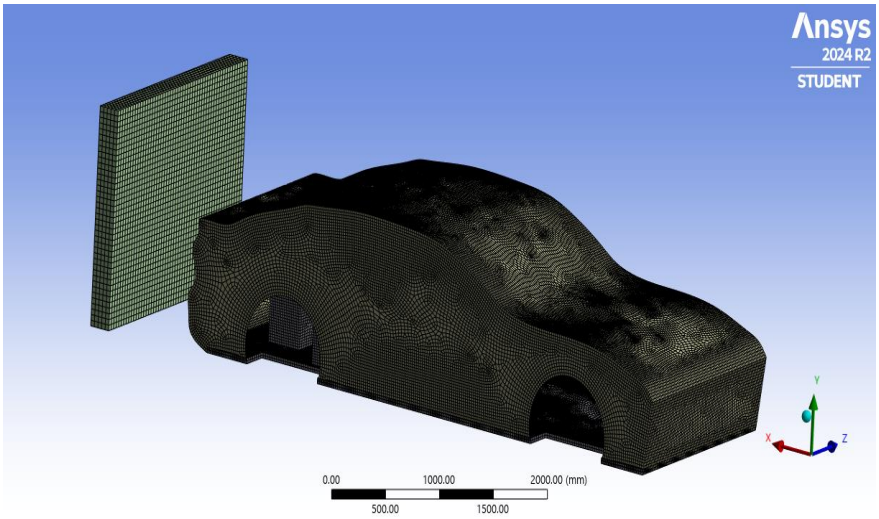

Figure 8.Meshed model of vehicle and wall (rear impact).

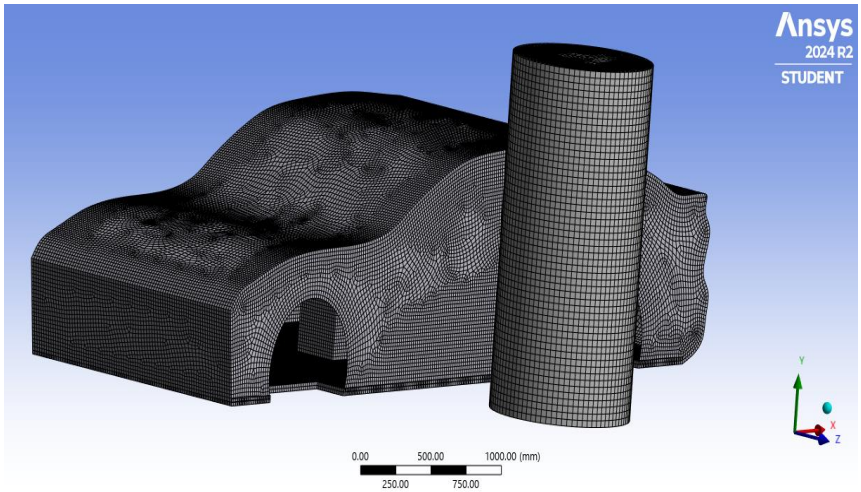

Figure 9. Meshed model of vehicle and wall (side impact).

2.2.Boundary conditions.

This section outlined the boundary and loading conditions applied to the vehicle. The first boundary condition was applied to the wall. Using the side impact scenario as a reference, Figures 10 and 11 showed the boundary conditions applied to the top and bottom faces of the cylindrical wall. This boundary condition ensures that the wall is a fixed support and can withstand the impact load of the vehicle as shown in Figure 12. This same condition is applied to the frontal and rear impact scenarios.

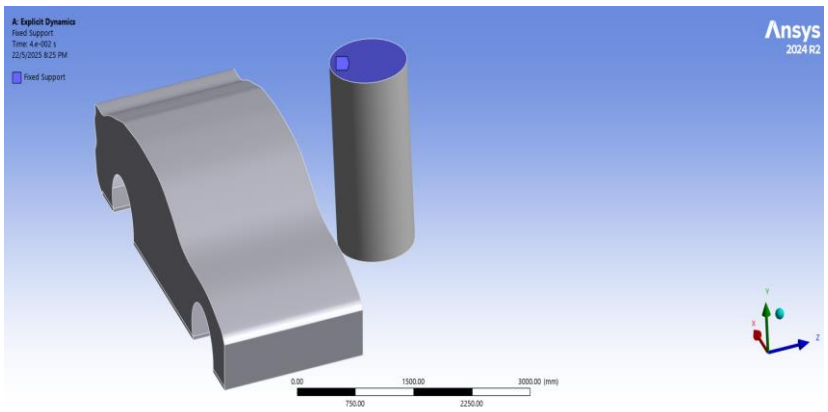

Figure 10. Boundary condition to wall (top face).

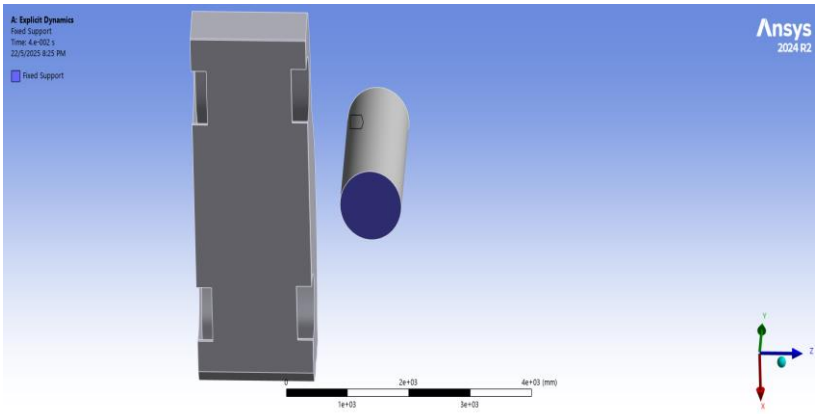

Figure11. Boundary condition to wall (bottom face).

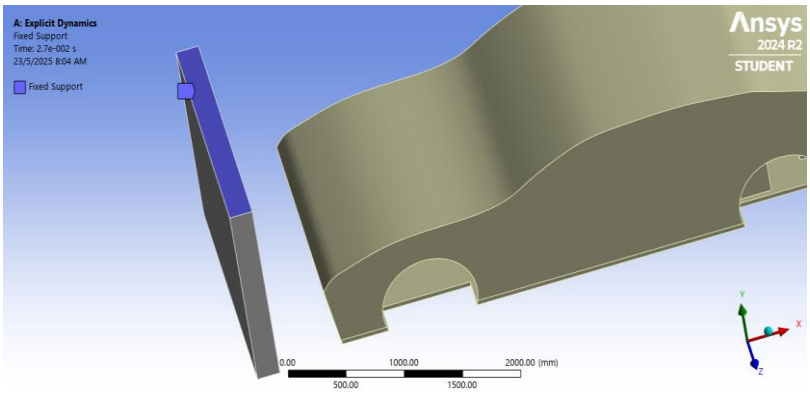

Figure 12. Fixed support boundary condition (frontal wall, top face).

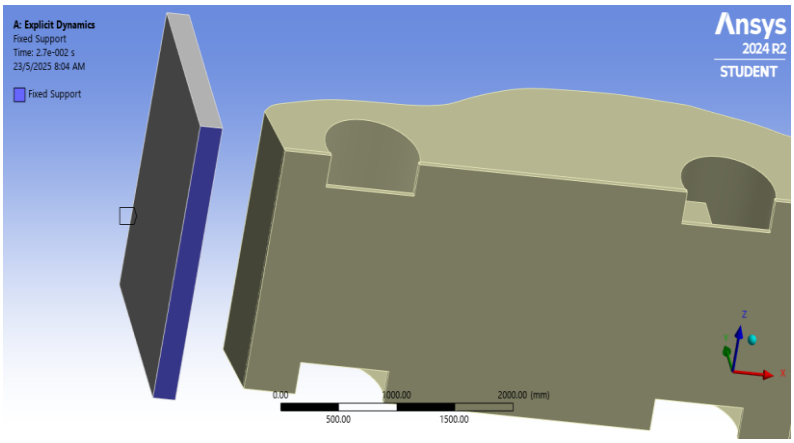

Figure 13. Fixed support boundary condition (frontal wall, bottom face).

The next boundary condition was applied to the body of the vehicle. The outline at the lower area of the car was the selected geometry for applying this condition, which was defined as a displacement. A total of 12 edges constituted the selected geometry. The displacement was defined in a coordinate system where the body was free to move along the X- and Z-axes but constrained in the Y-axis, simulating the real-life movement of a vehicle. The same condition was also applied to the hydrogen storage system. For the tanks, three faces of the cylinders were selected as the displacement geometry. The conditions were defined such that movement was free along the X- and Z-axes but constrained along the Y-axis. The impact scenarios considered to achieve the study objectives were listed in Table 4.

Table 4: Vehicle crash impact scenarios.

Collision Scenario	Testing Criteria
Frontal Impact	Testing of vehicle front impact collision
Side Impact	Testing of vehicle side impact collision
Rear Impact	Testing of vehicle rear impact collision

The boundary conditions of the vehicle model were defined as follows. A rigid concrete wall, representing the impact barrier, was set as a fixed support. The hydrogen storage tanks were assigned free displacement along the X- and Z-axes but were constrained along the Y-axis. An initial velocity of 23,777 mm/s (80 km/h) was applied along the X-axis, with the Y- and Z-axes constrained. The surface model of the vehicle was also allowed free displacement in the X- and Z-axes while constrained in the Y-axis, with the same initial velocity condition applied. Similarly, the chassis model was assigned free displacement in the X- and Z-axes but constrained along the Y-axis, together with the same velocity input. The defined vehicle speed followed NHTSA standards, while the hydrogen storage system layout was referenced from the second-generation Toyota Mirai. The velocity condition was set in the *Initial Conditions* module of ANSYS Mechanical, representing the speed at which the vehicle impacted the wall. This condition was applied consistently to the vehicle body, the hydrogen storage system, and the three storage tanks..

2.3.Material Behaviour & simulation tools of hydrogen storage tanks.

The hydrogen storage tank was assigned as a Type IV tank. In ANSYS, the material property of the three cylindrical models representing the hydrogen storage system was defined as polyethylene. The surrounding barriers were designed as supports, similar to those in a real vehicle, and the system was extended to represent the vehicle chassis for added protection. The simulation setup was defined through the following steps:

i. The crash scenarios for frontal, rear, and side impacts were simulated using the *Explicit Dynamics* tool in ANSYS.
ii. An adaptive time-step method was utilized, ensuring accurate results with respect to the desired collision speeds.
iii. To maintain energy balance with no loss or gain during the simulations, additional mesh refinement was applied using hourglass damping and tracking techniques..

3. Results and Discussion

To numerically analyse the results, the vehicle model with the hydrogen system must be developed and later meshed to have a discrete, simplified model. Figure 14-16 show the observed deformation of the vehicle after the simulation for frontal, rear and side impact

crash scenarios. The final simulation for all impact was an average of 0.037 seconds with a total of 46,025 cycles average value.

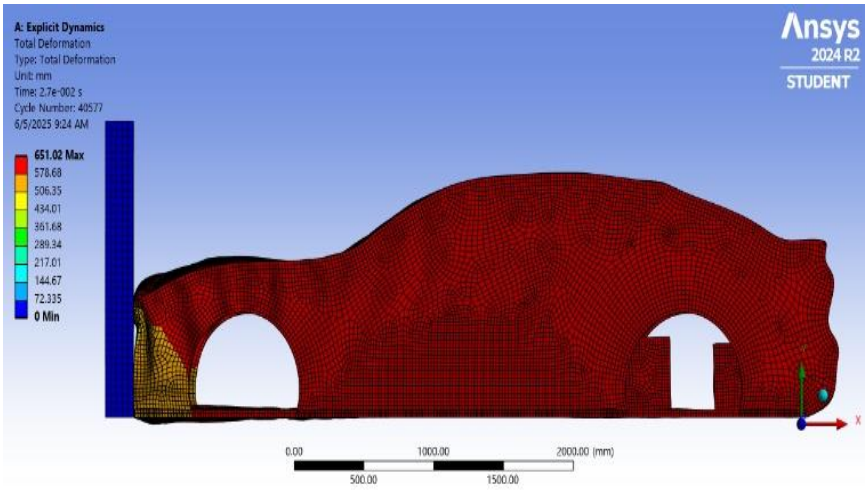

Figure 14. Observed deformation of vehicle (frontal impact).

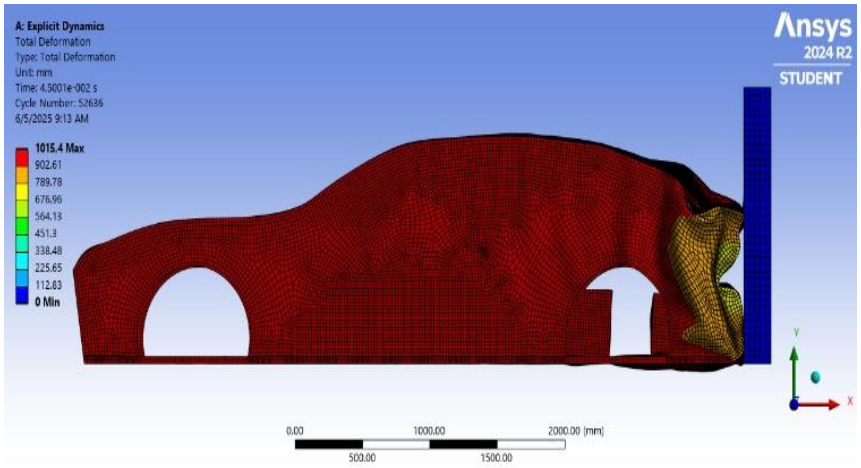

Figure 15. Observed deformation of vehicle (rear impact).

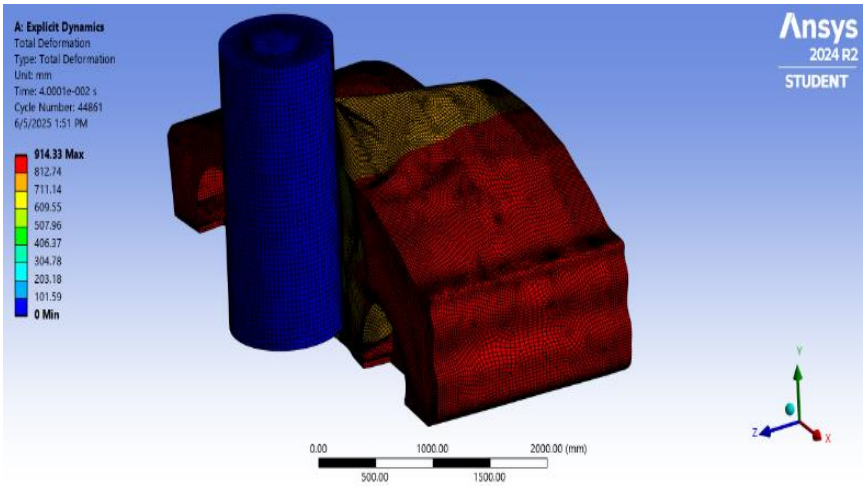

Figure 16. Observed deformation of vehicle (side impact).

The observed maximum value of deformation for the frontal impact was 651.02mm while for the rear impact value was 1015.4mm and side having 914.33mm. Looking further at the deformed shape of the vehicle, most of the deformation appears to take place at the points of first impact to the walls. Figure 17-19 show the observed deformation values of the hydrogen storage system after the simulation for frontal, rear and side impact crash scenarios. The final simulation for all impacts was an average 0.037 seconds with a total of 46,025 cycles average value.

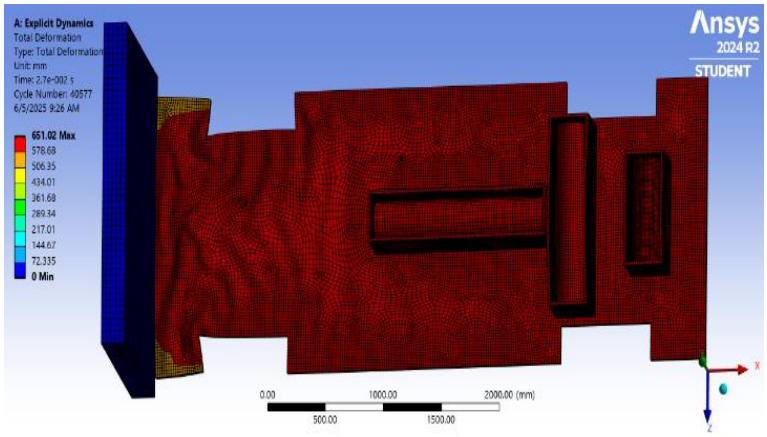

Figure 17. Observed deformation of hydrogen storage system (frontal impact).

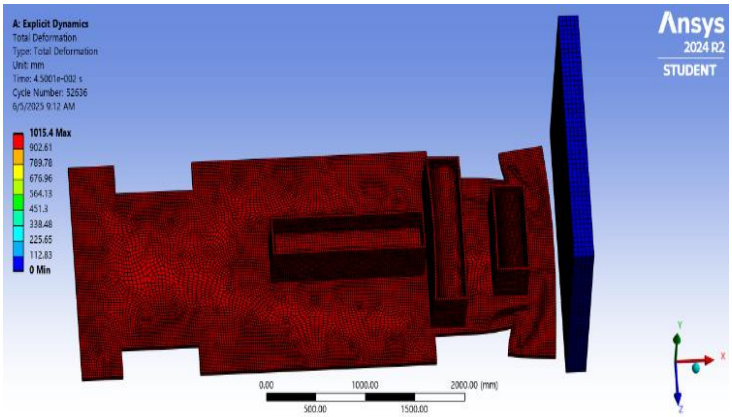

Figure 18. Observed deformation of hydrogen storage system (rear impact).

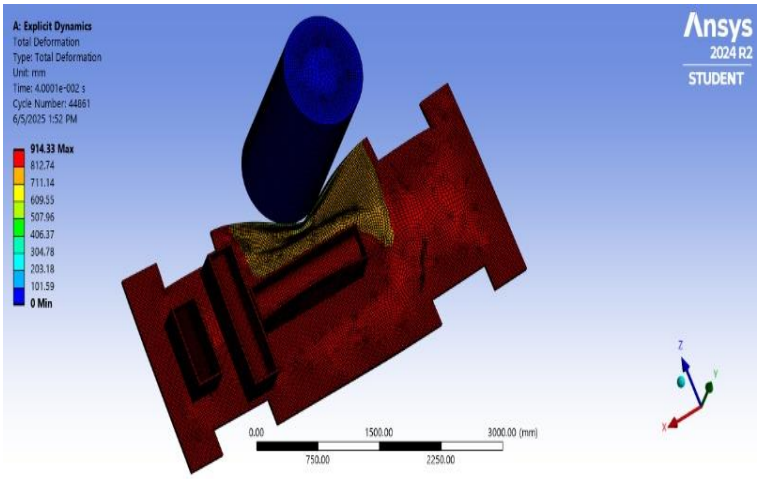

Figure19. Observed deformation of hydrogen storage system (side impact).

The simulation data revealed that the deformation shapes occurred primarily at the points of the vehicle that first made contact with the walls. Further analysis showed that, when comparing the frontal impact to the rear and side impacts, the hydrogen storage tanks were more likely to deform when the impacted wall was in closer proximity to the tanks. This trend was also reflected in the deformation patterns of the vehicle body, as illustrated in Figures 22, 23, and 24. A closer examination of the hydrogen storage system deformation in Figure 29 indicated a significant change in shape due to the reduced distance between the impacted wall and the tanks. Additionally, when comparing the deformation shape with the undeformed wireframe shown in Figure 21, it was evident that the hydrogen storage tanks underwent noticeable curvature, highlighting the severity of structural compromise during impact.

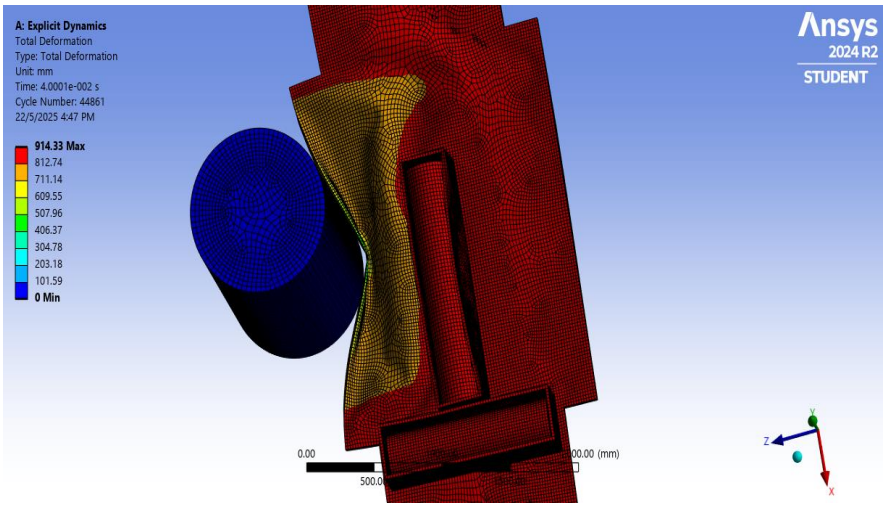

Figure 20. Observed deformation of hydrogen storage system (zoomed).

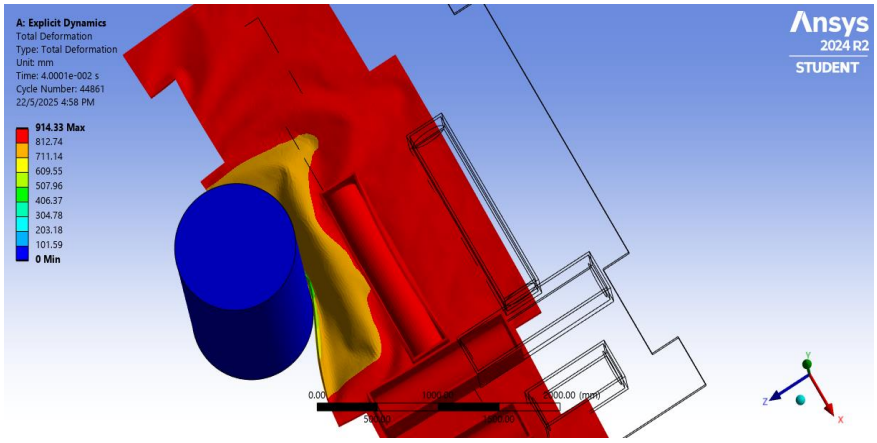

Figure 21. Undeformed wireframe of deformation.

The observed location of the tanks where the energy is absorbed after the simulation for frontal, rear and side impact crash scenarios, are shown in Figure 22-24. Each of the tanks are individually analysed for the amount of energy absorbed.

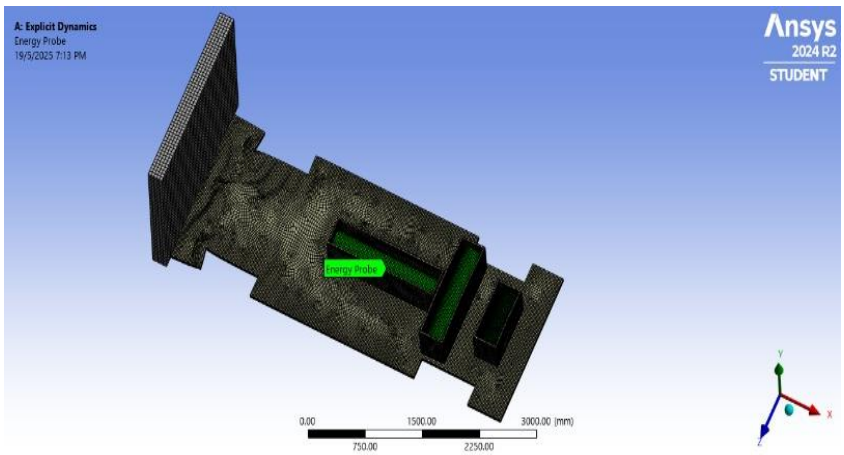

Figure 22. Observed energy probe (frontal impact).

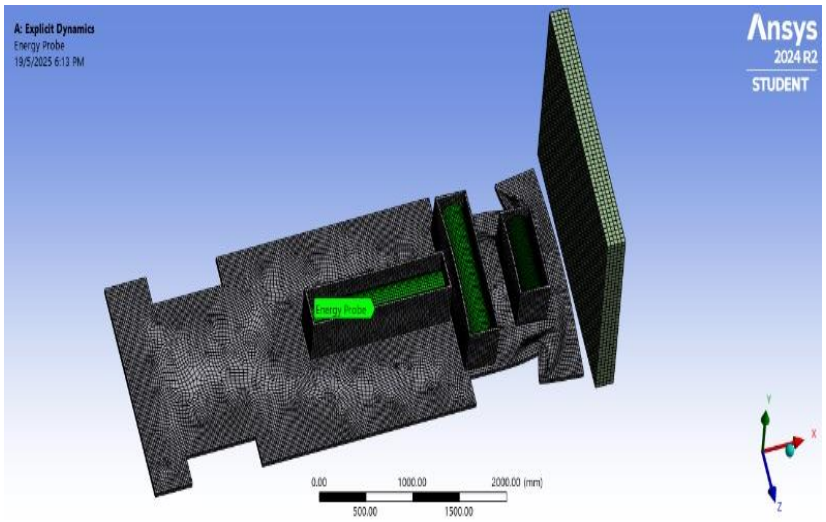

Figure 23. Observed energy probe (rear impact).

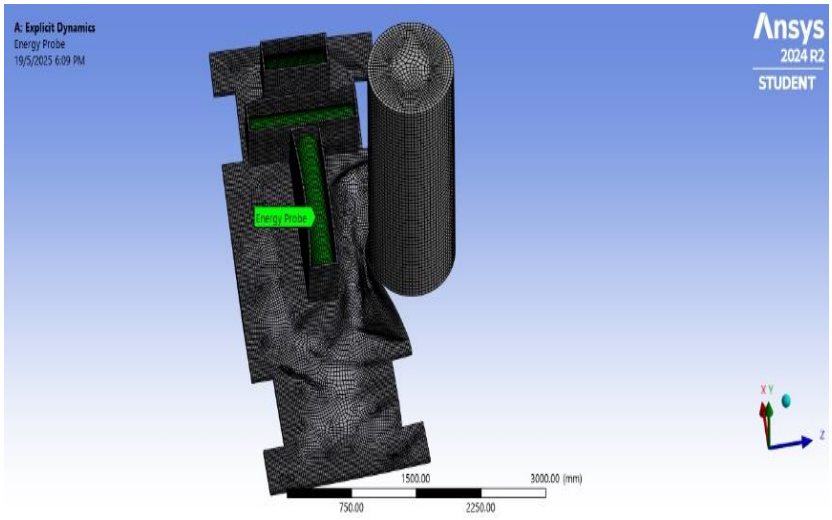

Figure 24. Observed energy probe (side impact).

From the frontal impact, the observed internal energy 88 J while the total energy was 49.2 KJ whereas the rear impact has internal energy of 110.2J with total energy of 55.03 KJ and internal energy value of 255.32 J with total energy of 55.05 J for side impact. Table 5

shows the summary of the data collected from the simulation for all three crash impact scenarios.

Table 3. Tabulated simulation results.

		Frontal Impact	Rear Impact	Side Impact
Deformation (mm)		651.02	1015.4	914.33
Equivalent Stress (MPa)		4630.2	3669.2	3356
Energy Absorbed	Internal (J)	88	110.2	255.32
	Total (J)	**49200**	**55030**	**55050**

Upon further investigation of the results, it was observed that the three crash scenarios produced varying figures of deformation, stress distribution, and energy absorption. The frontal impact showed the highest concentration of deformation at the front area of the vehicle, with a maximum deformation of 651.02 mm. The hydrogen storage system also experienced significant deformation, with peak stress values reaching 4630.2 MPa, which falls within the typical yield strength range of Type IV tanks. However, the internal energy absorbed by the tanks during the frontal crash was relatively low at 88 J, while the total system energy reached 49.2 kJ. This suggested that, despite the hydrogen tanks being subjected to high stress levels, most of the impact energy was dissipated throughout the vehicle body and its crumple zones. In comparison, the rear impact resulted in a higher deformation of 1015.4 mm in the vehicle body, although the stress levels in the hydrogen system were lower than those observed in the frontal impact. This displacement implied a greater risk to the hydrogen storage system due to its closer proximity to the rear of the vehicle. The internal energy absorbed during the rear impact was 110.2 J, with a total system energy of 55.03 kJ. For the side impact, a maximum deformation of 914.4 mm was recorded, but this scenario exerted a more critical effect on the hydrogen storage system. The tanks absorbed 255.32 J of internal energy, while stress levels reached 3356 MPa, indicating a highly localized loading that could compromise the integrity of the tanks. These findings suggested that the hydrogen storage system was most vulnerable in the side impact scenario, highlighting the need for additional protective measures. Furthermore, when the simulated results were compared to reported parameters for Type IV tanks, it was evident that the maximum stress values of 4630.2 MPa recorded during the frontal impact exceeded the typical thresholds. A detailed comparison of these values is presented in Table 6.

Table 4. Comparison of values reported from literature.

Parameter	Simulation			Values reported from literature
	Frontal Impact	Rear Impact	Side Impact	Thresholds
Maximum Deformation (mm)	651.02	1015.4	914.33	≥ 50 mm - Initial stages of cracking [6]
Equivalent Stress (MPa)	4630.2	3669.2	3356	≤ 2500 - Initial stages of cracking [9] ≥ 3000 MPa -Failure [10]
Internal Energy (J)	88	110.2	255.32	200-300 J
Total Energy (J)	**49200**	**55030**	**55050**	
Integrity of Tanks	**At Risk**	**At Risk**	**Compromised**	

The recorded equivalent stress levels surpassed those previously reported for Type IV hydrogen tanks, indicating a likelihood of failure in the hydrogen storage system. In addition to stress levels, the observed deformations suggested a serious compromise to the structure, as values greater than 50 mm exceeded the threshold. Notably, the side impact case

demonstrated the greatest risk to the hydrogen storage system in terms of stress concentration and energy absorption. This observation aligned with findings in the literature, which emphasized how tank configuration influences structural integrity.

The simulation results highlighted the vulnerability of hydrogen storage systems with high-pressure tanks, showing that the system was at risk of failure if not configured appropriately. Based on the results, several recommendations were made to improve the hydrogen storage system. First, the addition of a composite-reinforced layer was suggested, as composites provide high strength and can delay progressive tank failure. Literature indicates that Type IV tanks typically fail progressively; therefore, the use of thicker or hybrid composites could improve resistance to impact loading. Second, the tanks should be designed to withstand both internal and external pressures in the range of 35–70 MPa. This would enhance the realism of the simulation results and contribute to a more robust configuration of the hydrogen storage system. Overall, the most suitable configuration would be one in which the tanks were positioned strategically to balance protection with energy absorption during crash events.

4. Conclusions

The objective of this study was to numerically investigate the crashworthiness and safety of a hydrogen-powered vehicle in collision scenarios, with a focus on deformation, stress distribution, and energy absorption. Using ANSYS, a finite element model of a hydrogen-powered vehicle with a hydrogen storage system was developed. The vehicle was subjected to three impact modes: frontal, rear, and side impacts. The simulation results provided insights into the structural response of the vehicle under these impact scenarios. The findings revealed that the hydrogen system experienced significant deformation and elevated stress levels, with maximum stress values reaching 4630.2 MPa after a frontal impact—well above the typical threshold values for both the vehicle body and the hydrogen storage system. In the case of a side impact, the deformation and stresses resulted in high internal energy levels within the tanks, indicating a greater risk of structural failure. While the frontal impact posed a clear risk to the integrity of the hydrogen system, the side impact was more critical, as the concentrated energy load and reduced protective distance placed the tanks at greater risk of compromise. Regions prone to failure in the hydrogen storage system were identified, and these findings were consistent with observations reported in the literature. The results suggested that modifications to the vehicle model and hydrogen storage system would be valuable for gaining a deeper understanding of system behavior under collision conditions. Such modifications could include the addition of further boundary conditions and analysis settings. For example, applying internal load pressure would allow for a more realistic representation of tank behavior under crash scenarios, thereby enabling a more comprehensive failure analysis. Given the computational capabilities of finite element analysis (FEA) tools, future studies could also incorporate advanced material failure criteria to enhance predictive accuracy. These may include limits such as plastic strain, progressive damage models, or zone-based modeling. Although the present study did not include internal tank pressure or more detailed failure modes, the simulations nonetheless provided valuable insights into safety considerations for hydrogen-powered vehicle design. These findings contribute to the ongoing development of safer and more sustainable clean energy transportation solutions.

Acknowledgments

The authors would like to show appreciation to Curtin University Malaysia for the utilization of lab facilities and software license and funding for this study.

Author Contribution

The specific contributions of the authors to this study were as follows: Conceptualization was carried out by Chipego J. and Kyaw M.A.; methodology was developed by Kyaw M.A.; data collection was performed by Chipego J.; data analysis was conducted by Sujan D.; the manuscript was written by Kyaw M.A.; supervision was provided by Kyaw M.A.; and funding acquisition was also undertaken by Kyaw M.A.

Competing Interest

The authors declare that they have no known competing financial interests or personal relationships that could have appeared to influence the work reported in this paper.

References

[1] Hassan, Q.; Azzawi, I.D.J.; Sameen, A.Z.; Salman, H.M. (2023). Hydrogen fuel cell vehicles: Opportunities and challenges. *Sustainability (Switzerland)*, *15*(15). https://doi.org/10.3390/su151511501.

[2] Thomas, C.E. (1996). Preliminary hydrogen vehicle safety report. Prepared by Directed Technologies, Inc. for Ford Motor Company, contract No. DE-AC02-94CE50389, U.S. Department of Energy.

[3] Swain, M.R.; Swain, M.N. (1992). A comparison of H2, CH4, and C3H8 fuel leakage in residential settings. *International Journal of Hydrogen Energy*, *17*(10), 807–815.

[4] Barbir, F. (n.d.). Safety issues of hydrogen in vehicles. Energy Partners, 1501 Northpoint Pkwy, #102, West Palm Beach, FL 33407, U.S.A.

[5] Sazali, N.; Wan Salleh, W.N.; Jamaludin, A.S.; Mhd Razali, M.N. (2020). New perspectives on fuel cell technology: A brief review. *Membranes*, *10*(5). https://doi.org/10.3390/membranes10050099.

[6] Changala, P.B.; Nguyen, T.L.; Baraban, J.H.; Ellison, G.B.; Stanton, J.F.; Bross, D.H.; Ruscic, B. (2017). Active thermochemical tables: The adiabatic ionization energy of hydrogen peroxide. *Journal of Physical Chemistry A*, *121*(46), 8799–8806. https://doi.org/10.1021/acs.jpca.7b06221.

[7] Deng, B.; Zhou, L.; Jiang, Z.; Jiang, Z.J. (2019). High catalytic performance of nickel foam supported Co2P-Ni2P for overall water splitting and its structural evolutions during hydrogen/oxygen evolution reactions in alkaline solutions. *Journal of Catalysis*, *373*, 81–92. https://doi.org/10.1016/j.jcat.2019.03.038.

[8] Gurz, M.; Baltacioglu, E.; Hames, Y.; Kaya, K. (2017). The meeting of hydrogen and automotive: A review. *International Journal of Hydrogen Energy*, *42*(36), 23334–23346. https://doi.org/10.1016/j.ijhydene.2017.02.124.

[9] Yang, R.; Zhang, W.; Li, S.; Xu, M.; Huang, W.; Qin, Z. (2023). Finite element analysis and optimization of hydrogen fuel cell city bus body frame structure. *Applied Sciences (Switzerland)*, *13*(19). https://doi.org/10.3390/app131910964.

[10] Idrees, U.; Ahmad, S.; Shah, I.A.; Talha, M.; Shehzad, R.; Amjad, M.; Koloor, S.S.R. (2023). Finite element analysis of car frame frontal crash using lightweight materials. *Journal of Engineering Research*, *11*(1), 100007. https://doi.org/10.1016/j.jer.2023.100007.

[11] Zhu, J.; Li, Y.; Cao, W.; Li, Y.; Gao, Z. (2023). Failure analysis of novel BOSS structures for Type IV hydrogen storage vessels. *Energies*, *16*(10), 4005. https://doi.org/10.3390/en16104005.
[12] Zhu, S.; Ding, C.; Hu, X.; Tian, Y. (2024). Analysis of safety technical standards for hydrogen storage in fuel cell vehicles. *Frontiers in Energy Research*, *12*. https://doi.org/10.3389/fenrg.2024.1376739.